

One-time measurement to characterize complex amplitude single component in symmetry superposed optical vortices

CHEN WANG,^{1,2} YUAN REN,^{1,2,*} TONG LIU^{1,3} ZHENGLIANG LIU,^{1,2} SONG QIU,^{1,2} YOU DING,^{1,2} RUIJIAN LI,^{1,2} AND JIE ZHAO,^{1,2}

¹ Department of Aerospace Science and Technology, Space Engineering University, Beijing 101416, China

² Lab of Quantum Detection & Awareness, Space Engineering University, Beijing 101416, China

³ State Key Lab of Laser Propulsion & its Application, Space Engineering University, Beijing 101416, China

* renyuan_823@aliyun.com

Abstract: Complex amplitude measurement is an essential prerequisite for light field characterization. In this work, we propose a one-time measurement method to characterize the complex amplitude of symmetry superposed optical vortices (SSOVs) with only one picture registered by CCD. This method includes two strategies we proposed. One is the ring extraction strategy for amplitude measurement, and another is the rotational measurement strategy for phase measurement. In the proof-of-concept experiment, the complex amplitude is characterized, and the mode purity is well measured. This method has excellent flexibility, rapidity, and robustness, which can be applied to various occasions and harsh conditions. Careful alignment and optimized error analysis allow us to generate and measure a single component with mode purity as high as 99.99%. © 2020 Optical Society of America

© 2020 Optical Society of America under the terms of the [OSA Open Access Publishing Agreement](#)

1. INTRODUCTION

In 1992, Allen *et al.* proved that an optical vortex (OV) whose complex amplitude comprises the helical term $\exp(im\theta)$ carries an orbital angular momentum (OAM) per photon of $m\hbar$ [1], which has aroused widespread concern among researchers [2-17], where m denotes the topological charge (TC), θ represents the azimuthal angle and \hbar is the reduced Planck constant. Since then, OVs have been utilized in a plethora of applications in the field of optical micro-manipulation[18, 19], plasmonics[20, 21], rotation probing[22-28], optical communication[29-31], gravitational wave detection[32, 33] and so on. The symmetry superposed OVs (SSOVs) are often used here instead of a single component. Before practical application, we need to characterize the complex amplitude of a single component in SSOVs and measure its mode purity. It is an essential quality reference for an OV, which determines OV's performance in various applications. In the rotating Doppler effect[34, 35], low mode purity means frequency spectrum expansion, significantly increasing signal detection difficulty. In the field of micro-manipulation, high mode purity is more conducive to the use of superposed OVs to achieve static capture of particles[36].

Many demonstrated methods characterize and measure the mode purity of SSOVs[37-45]. But the most versatile approach is to resolve a field into a coherent sum of modes, each with a particular amplitude weighting and phase: a so-called modal decomposition[46]. However, we need to use an SLM to scan multiple holograms one by one to complete the measurement. Is there a way to characterize the complex amplitude of SSOVs with only one-time measurement to improve measurement efficiency? The answer is yes. Recent work showed that the phase-shifting holography in an interferometer could be used to measure the mode purity of OVs[47]. This work required a separate reference path that increased the setup's complexity and

introduced additional phase noise. In 2019, Andersen *et al.* modified the work mentioned above to achieve the same goal with only one path[48]. However, these two works need multiple measurements to characterize the complex amplitude of the aimed optical field.

In this work, we propose a one-time measurement method to characterize the complex amplitude of SSOVs with only one picture registered by CCD based on phase-shifting technology, which is reported for the first time. We can use this method to evaluate the quality of the generated SSOVs. This method includes two strategies we proposed. One is the ring extraction strategy for amplitude measurement, and another is the rotational measurement strategy for phase measurement. This method takes a short time, and we can characterize the complex amplitude of the SSOVs and achieve the measurement of mode purity in only 0.24 seconds. Since we use part of the SSOVs to be measured as the reference light, though we use the phase-shifting technology, no additional reference beams are required for interference anymore, which has not been reported before.

2. THEORY AND METHODS

A PHASE-SHIFTING THEORY OF SSOVS

The self-interference method requires four intensities $I(x, y; \phi_s)$ of SSOVs. ϕ_s denotes the shifting phase of one single component. We only consider that the SSOVs only have two symmetry components for simplicity without loss of generality.

May the two components of SSOVs be

$$\begin{aligned} E_1 &= A_1 \exp(i\phi) \exp(i\phi_s) \\ E_2 &= A_2 \exp(-i\phi) \end{aligned} \quad (1)$$

where $\phi_s = 0, \pi/2, \pi, 3\pi/2$. The four intensity distributions of SSOVs are:

$$\begin{aligned} I_0(x, y; 0) &= I'(x, y) + I''(x, y) \cos(2\phi); \quad I_0(x, y; \pi/2) = I'(x, y) - I''(x, y) \sin(2\phi) \\ I_0(x, y; \pi) &= I'(x, y) - I''(x, y) \cos(2\phi); \quad I_0(x, y; 3\pi/2) = I'(x, y) + I''(x, y) \sin(2\phi) \end{aligned} \quad (2)$$

where $I'(x, y) = A_1^2 + A_2^2$, $I''(x, y) = 2A_1A_2$. Consequently, we can calculate the phase ϕ :

$$\phi = \frac{1}{2} \tan^{-1} \left[\frac{I_0(x, y; 3\pi/2) - I_0(x, y; \pi/2)}{I_0(x, y; 0) - I_0(x, y; \pi)} \right] \quad (3)$$

Although the intensity of the two components does not affect the final result, according to interference contrast:

$$\gamma = \frac{I_{\max} - I_{\min}}{I_{\max} + I_{\min}} \quad (4)$$

we set the two equals to get the best interference pattern. Where

$$I_{\max} = A_1 + A_2; \quad I_{\min} = A_1 - A_2 \quad (5)$$

B ENCODING HOLOGRAM

In this part, we briefly introduce the process of encoding the hologram to generate SSOVs. We use the technique demonstrated in ref.[49, 50] to encode the hologram. The hologram can be used to achieve complex amplitude modulation of incident light on a phase-only SLM. The process of encoding the hologram is shown in Fig. 1. The expression of the hologram is:

$$\phi_{hol} = F(I_{ss}) \sin(\phi_{ss} + \phi_{gra}) \quad (6)$$

where I_{ss} denotes the normalized amplitude of SSOVs, $F(I_{ss})$ is the numerical inversion result of the first-order Bessel function of I_{ss} in $[0, 1.84]$, ϕ_{ss} represents the phase of SSOVs, and ϕ_{gra} is the blazed grating phase. The blazed grating prevents part of the unmodulated light from mixing into the required SSOVs, diffracting the required light beam to the first order, and

leaving the unmodulated light in the zero-order. The unmodulated light is due to the gaps in the SLM liquid crystal arrangement. Although using an SLM for complex amplitude modulation sacrifices phase depth, it allows us to radially modulate the incident light field to generate an eigenmode of SSOVs instead of hypergeometric mode[51]. Load the encoded hologram onto the SLM, and we can get the intensity $I_0(x, y; 0)$ of SSOVs.

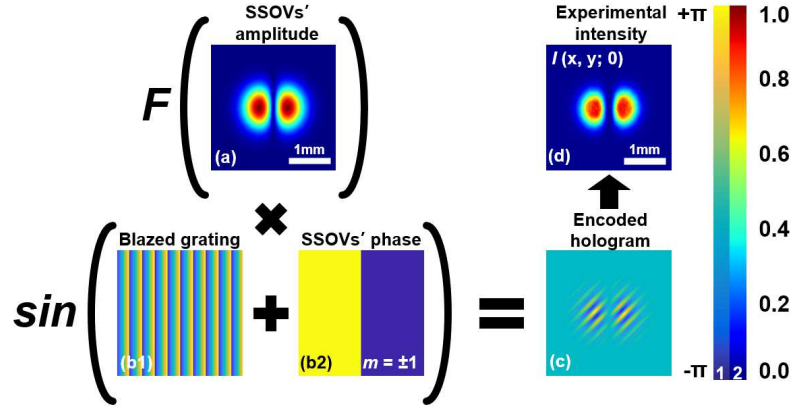


Fig. 1 Schematic representation of encoding the hologram. The TCs of SSOVs here are ± 1 . (a) The normalized amplitude of the SSOVs. (b1) The phase of a blazed grating. (b2) The phase of the SSOVs. (c) Encoded hologram. (d) The experimental intensity $I_0(x, y; 0)$ of the SSOVs generated by (c). The color bar 1 indicates the phase range. The color bar 2 shows the range of (a) and (d).

C RING EXTRACTION AND ROTATIONAL MEASUREMENT STRATEGY

To obtain the complex amplitude of SSOVs through one measurement, we propose two strategies. One is the ring extraction strategy for amplitude measurement, and another is the rotational measurement strategy for phase measurement.

In the ring extraction strategy, we consider a typical OV called the Laguerre-Gaussian (LG) beam. In this case, the amplitudes in Eqs.(1) are:

$$A(x, y) = A_1 = A_2 = \sqrt{\frac{2p!}{\pi(p+|m|)!}} \left(\frac{r\sqrt{2}}{\omega_0}\right)^{|m|} \exp\left(-\frac{r^2}{\omega_0^2}\right) L\left(\frac{2r^2}{\omega_0^2}\right) \quad (7)$$

where $r = \sqrt{x^2 + y^2}$, p represents the radial node, ω_0 is the waist radius, and L denotes the Laguerre polynomial. The initial interference intensity in Eqs.(2) turns to:

$$I_0(x, y; 0) = 2A^2(x, y) + 2A^2(x, y) \cos(2\phi) \quad (8)$$

where

$$I_{0\max} = 4A^2 \quad (\phi = \pi n, n \in Z) \quad (9)$$

It can be seen from the Eqs.(9) that interference affects the angular distribution of SSOVs, but the light intensity before interference can always be restored in the radial direction (divide $I_{0\max}$ by 4), which makes it possible to restore the original single-component intensity through interference intensity by extracting the maximum intensity in rings in the radial direction. In the actual extraction, we do not need to divide $I_{0\max}$ by four because we will also normalize the entire intensity value when all extractions are over. Schematic representation of the ring extraction strategy is shown in Fig. 2 (a1-a4). In the interference intensity registered by CCD, we take multiple rings at equal intervals d in the radial direction. In each ring, we take the maximum intensity in the ring and assign this value to the ring's corresponding spatial position.

As the interval gradually decreases, the restored intensity distribution is closer to the original single component in SSOVs, as depicted in Fig. 2 (a2-a4).

In the rotational measurement strategy, we replace the actual phase-shifting operation by rotating the picture shown in Fig. 2 (b1). A schematic representation of the rotational measurement strategy is shown in Fig. 2 (a1-a4). Through a simple rotation operation, we can quickly obtain the four interference intensities required by Eqs.(2). It should be noted that the corresponding rotational angle of high-order SSOVs should be $45/m$ degrees, $90/m$ degrees, and $135/m$ degrees, where m denotes TCs of a single component in high-order SSOVs.

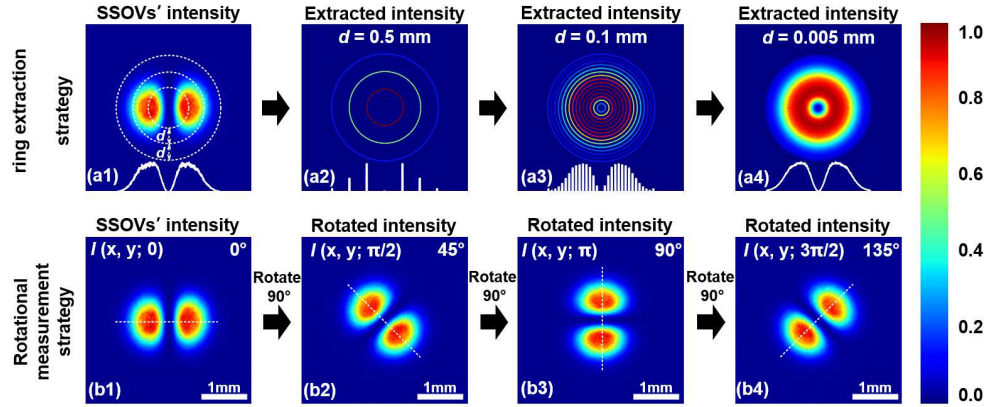


Fig. 2 Schematic representation of (a1-a4) the ring extraction strategy and (b1-b4) the rotational measurement strategy. The TCs of SSOVs here are ± 1 . (a1) SSOVs' intensity registered by CCD. White dotted lines denote the extracting and filling position. (a2-a4) Extracted intensities with $d = 0.5\text{mm}$, $d = 0.1\text{mm}$, and $d = 0.005\text{mm}$, respectively. (b1) SSOVs' intensity registered by CCD. (b2-b4) Rotated intensities at 45 degrees, 90 degrees, and 135 degrees, respectively. White dotted lines denote the axis of symmetry.

D CALCULATING THE PHASE OF SINGLE COMPONENT IN SSOVS

Theoretically speaking, after obtaining four intensity distribution results, the desired phase can be deduced inversely. However, due to trigonometric functions' introduction, the desired phase is wrapped into 2π in the actual calculation. We cannot get the desired result by simply dividing by 2, as shown in Eqs.(3). Consequently, the phase unwrapping technology is required[52]. Firstly, we need to trim the phase to achieve maximum phase unwrapping efficiency, as depicted in Fig. 3 (b) and Fig. 3 (c). Finally, we can get the unwrapping phase by employed the phase unwrapping technology shown in ref.[52], as depicted in Fig. 3 (e1) and Fig. 3 (e2). What is implemented here is not phase unwrapping in the traditional sense: the phase is restored to a linear increase. The purpose of phase unwrapping here is to restore the phase to one-half of the calculated phase after Fig. 3 (b). We can directly perform phase unwrapping or perform windowed Fourier transform[53] (WFT) first and then perform phase unwrapping. The WFT is adopted here to filter the trimmed phase to reduce noise further and smooth the phase. The unwrapped phase obtained directly in the laboratory environment is ideal, but it does not mean that good results are maintained under complex conditions such as outdoors. Therefore, The WFT is optional according to the actual situation.

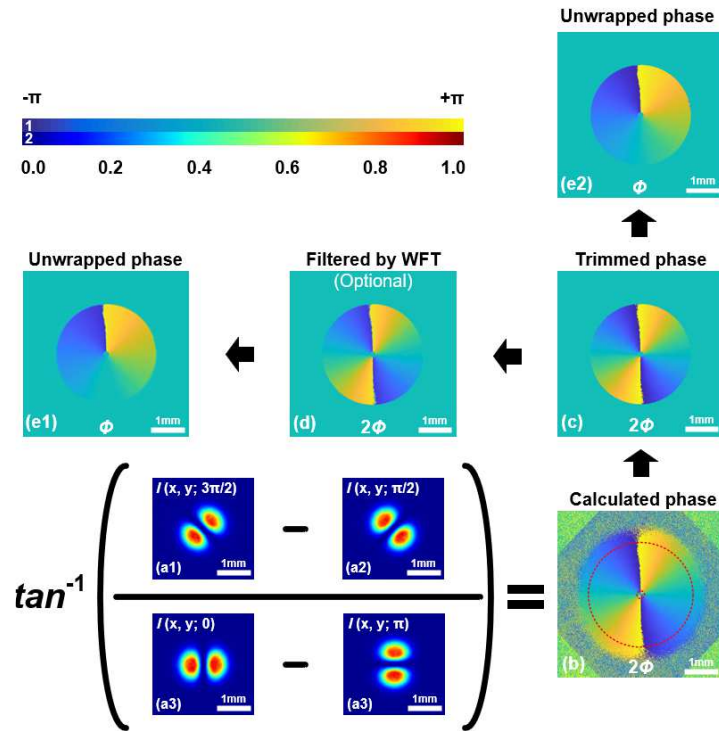


Fig. 3 Schematic representation of calculating required phases. The TCs of SSOVs here are ± 1 . (a1-a4) four rotated intensities SSOVs. (b) Calculated phase. The red dotted lines indicate the trimming area. (c) Trimmed phase. (d) Trimmed phase filtered by WFT (optional). (e1-e2) Unwrapped phase. The color bar 1 indicates the phase range. The color bar 2 indicates the range of intensities.

3. EXPERIMENTAL RESULTS

The experimental setup employed to generate a PPOV is shown in Fig. 4. The laser (NEWPORT N-LHP-151) delivers a collimated Gaussian beam with a wavelength of 632.8nm after a linear polarizer (LP), a half-wave plate (HWP), and a telescope consisting of two lenses (L1, L2) are used for collimation. The combination of the LP and the HWP is served to rotate the laser polarization state along the SLM's long display axis and adjust the incident light's power on SLM. The SLM (UPOLABS HDLSLM80R) precisely modulates the incident light via loading a hologram mentioned above. The aperture (AP) is then used to select the beam's first diffraction order to avoid other stray light. A CCD camera (NEWPORT LBP2) registers the intensity pattern after L4.

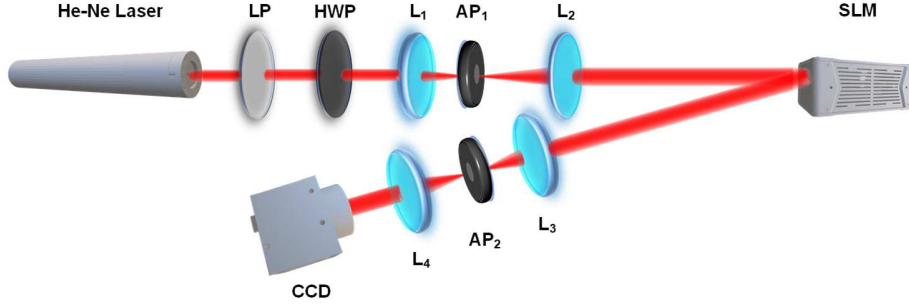


Fig. 4 Experimental setup for measuring mode purity of single component in superposed OV. LP: linear polarizer. HWP: half-wave plate. L: lens. SLM: spatial light modulator. AP: aperture. CCD: charge-coupled device.

Experimental results of one-time measurement are shown in Fig. 5. In the proof-of-concept experiment, we select four typical SSOVs (one order, low order, high order, and radial node) to characterize the complex amplitude with only one picture registered by CCD shown in Fig. 5 (a1-d1). We obtain the intensity distributions of a single component in SSOVs through the ring extraction strategy, as shown in Fig. 5 (a3-d3). We get the phase distributions of a single component in SSOVs by rotational measurement strategy after unwrapping.

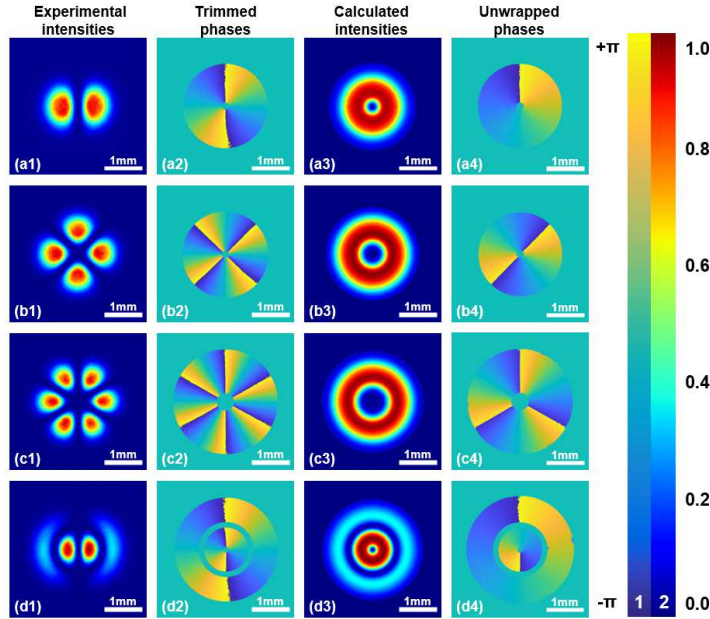


Fig. 5 Experimental results of one-time measurement. (a1-d1) Interference intensities of SSOVs. The TCs are ± 1 , ± 2 , ± 3 , and ± 1 , respectively. The radial node in (d1) is 1. (a2-d2) Calculated phases after trimming. (a3-d3) Calculated intensities. (a4-d4) Unwrapped phases. The color bar 1 indicates the range of intensities. The color bar 2 indicates the phase range.

To prove the accuracy of the detection method, we selected two SSOVs to calculate the mode purity. The mode purity for an arbitrary field Ψ can be calculated with[54, 55]:

$$\Gamma_p = \frac{\sum_{m=-\infty}^{+\infty} C_m^p}{\sum_{p=0}^{+\infty} \sum_{m=-\infty}^{+\infty} C_m^p}, \Gamma_m = \frac{\sum_{p=0}^{+\infty} C_m^p}{\sum_{p=0}^{+\infty} \sum_{m=-\infty}^{+\infty} C_m^p} \quad (10)$$

where

$$C_m^p = \int_0^\infty \langle a_m^p(r, \phi, z) | a_m^p(r, \phi, z) \rangle r dr \quad (11)$$

$$a_m^p(r, z) = 1 / (2\pi)^{1/2} \int_0^{2\pi} \Psi(r, \phi, z) \text{LG}_p^m d\phi \quad (12)$$

where LG_p^m denotes the LG beam. The calculated mode purity of a single component is shown in Fig. 6. Whether it is radial decomposition or angular decomposition, the model purity can be calculated by the one-time measurement method. Experimental results show that the angular mode's purity (OAM spectrums) is higher than that of the radial mode (radial distributions), consistent with the more robustness of the angular distribution of an OV.

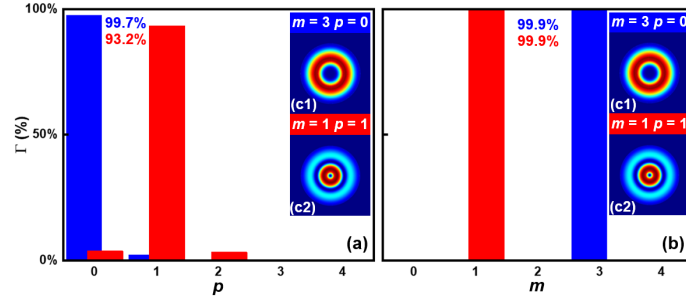


Fig. 6 Experimental distributions of single component mode purity. (a) Radial distributions and (b) OAM spectrums of $m=3$ ($p=0$) and $m=1$ ($p=1$) from SSOVs $m=\pm 3$ ($p=0$) and $m=\pm 1$ ($p=1$), respectively.

4. DISCUSSION

A ANGULAR ERROR

Firstly, we demonstrate the rotational measurement strategy's angular errors (new strategy) compared with the phase-shifting method (old method using four interferograms). The experimental results are depicted in Fig. 7. In the phase measurement of a single component in SSOVs, the low-order OV phase restored using the new strategy has a significant offset compared with the old method, as shown in Fig. 7 (a). However, the measured model purity is not much different. In the phase measurement of high-order OV, excellent performance in both phase distribution and measurement results are shown in Fig. 7 (b). The experimental results show the accuracy and robustness of the rotational measurement strategy.

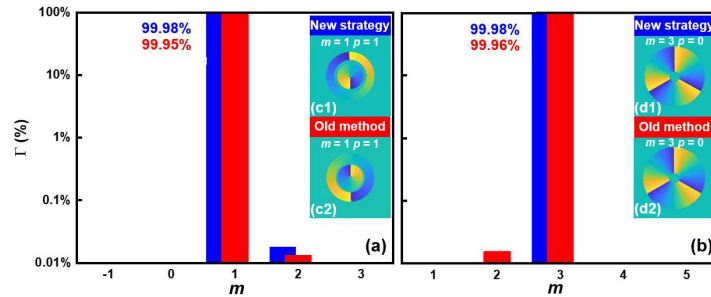


Fig. 7 Comparison of the rotational measurement strategy (new strategy) with the phase-shifting method (old method) on the measurement of OAM spectrums. (a) OAM spectrums of $m=1$ ($p=1$). (b) OAM spectrums of $m=3$ ($p=0$).

B RADIAL ERROR

Secondly, we'd like to show the radial errors introduced by interval d in the ring extraction strategy. The interval d determines the restored degree of the intensity distribution. As the interval d decreases, the intensity distribution is closer to the ideal situation (red line), as shown in Fig. 8 (a). Interestingly, although the interval affects the restored intensity distribution, it has little effect on the measurement results of model purity, which fully demonstrates this method's robustness, as shown in Fig. 8 (b) and (c).

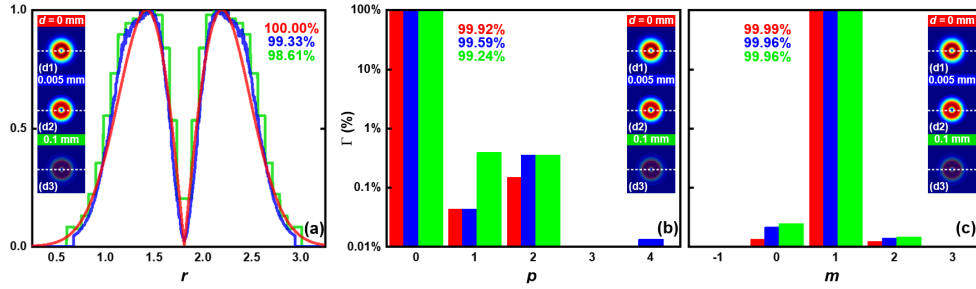


Fig. 8 The radial errors introduced by interval d in the ring extraction strategy. The TC is 1 and the radial node is 0 here. (a) Intensity distribution curves intercepted at the white dotted lines shown in (d1-d3). The number identified in the upper right corner identifies the correlation coefficient between the current intensity distribution and the ideal intensity distribution of the single component in SSOVs. (b) Radial distributions. (c) OAM spectra. (d1) Ideal intensity distribution with $d = 0.005\text{mm}$. (d2) Restored intensity distribution with $d = 0.005\text{mm}$. (d3) Restored intensity distribution with $d = 0.1\text{mm}$.

C EXPERIMENTAL ERROR

Finally, we demonstrate the effect of experimental errors on the measurement. One is the effect of different exposure times on the measurement. The results show that as the exposure time increases, the measured mode purity decreases slightly, as shown in Fig. 9 (a). This can be explained that without affecting the sampling, the increase in exposure time causes the image's noise to increase, so the mode purity is slightly reduced. Another is the effect of CCD tilt on the measurement. The results show that as the CCD tilt increases, the measured mode purity decreases somewhat, as shown in Fig. 9 (a). This can be explained that the tilt of CCD affects the symmetry distribution of SSOVs, which affects the accuracy of the phase calculation, as shown in Fig. 9 (b). The third one is the effect of the CCD shift on the measurement. The results show that as the CCD shift increases, the measured mode purity decreases slightly, as shown in Fig. 9 (c). Although the CCD shift does not change the SSOVs' distribution, if we still perform mode decomposition at the position shown in 0 pixels, the mode decomposition's accuracy will be reduced. The above three experimental errors cause 0.1% to 0.01% deviation of the measured mode purity. But overall, the experimental results show that the self-interference method has excellent robustness. Careful alignment and optimized error analysis allow us to generate and measure a single component with mode purity as high as 99.99%.

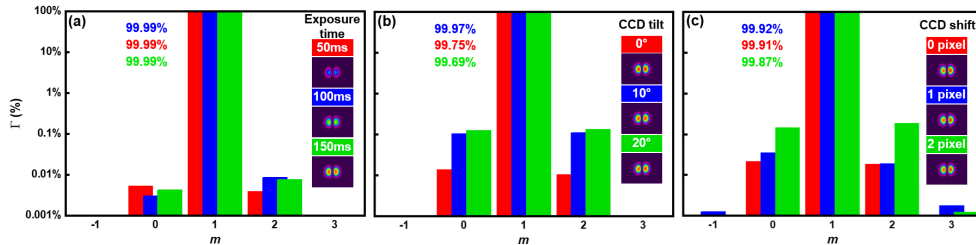


Fig. 9 The effect of the experimental error on the results. The effect of (a) exposure times, (b) CCD tilt, and (c) CCD shift on the measurement of the mode purity.

5. CONCLUSION

In summary, we propose a one-time measurement method to characterize the complex amplitude of SSOVs with only one picture registered by CCD based on phase-shifting technology, which is reported for the first time. Firstly, we introduce the phase-shifting theory of SSOVs. Secondly, we demonstrate the process of encoding the hologram. Thirdly, we demonstrate two strategies we proposed. One is the ring extraction strategy for amplitude measurement, and another is the rotational measurement strategy for phase measurement. Fourthly, we show the process of calculating the phase of a single component in SSOVs. In the proof-of-concept experiment, the complex amplitude is characterized, and the mode purity is well measured. Finally, we demonstrate the angular and radial errors on the experimental results and discuss the effect of experimental error of exposure time, CCD tilt, and CCD shift. The experimental results indicate that the one-time measurement has excellent flexibility, rapidity, and robustness, which can be applied to various occasions and harsh conditions.

Funding

This work was supported in part by the National Nature Science Foundation of China under Grant 11772001 and 61805283, and in part by the Key research projects of the foundation strengthening program and Outstanding Youth Science Foundation.

Disclosures

The authors declare no conflicts of interest.

References

1. L. Allen, M. W. Beijersbergen, R. J. Spreeuw, and J. P. Woerdman, "Orbital angular momentum of light and the transformation of Laguerre-Gaussian laser modes," *Physical Review A Atomic Molecular & Optical Physics* 45, 8185 (1992).
2. L. Chen, W. Zhang, Q. Lu, and X. Lin, "Making and identifying optical superpositions of high orbital angular momenta," *Physical Review A* 88(2013).
3. X. Li, Y. Tai, F. Lv, and Z. Nie, "Measuring the fractional topological charge of LG beams by using interference intensity analysis," *Optics Communications* 334, 235-239 (2015).
4. S. Fu, C. Gao, Y. Shi, K. Dai, L. Zhong, and S. Zhang, "Generating polarization vortices by using helical beams and a Twyman Green interferometer," *Opt Lett* 40, 1775-1778 (2015).
5. X. Ke and G. Tian, "Experiment on Generation of Vortex Light with Few-Mode Fiber," *Chinese Journal of Lasers* 44(2017).
6. H. Ma, X. Li, Y. Tai, H. Li, J. Wang, M. Tang, Y. Wang, J. Tang, and Z. Nie, "In situ measurement of the topological charge of a perfect vortex using the phase shift method," *Opt Lett* 42, 135-138 (2017).
7. X. Qiu, F. Li, W. Zhang, Z. Zhu, and L. Chen, "Spiral phase contrast imaging in nonlinear optics: seeing phase objects using invisible illumination," *Optica* 5, 208 (2018).
8. D. Yang, Y. Li, D. Deng, Q. Chen, Y. Zhang, Y. Liu, J. Gao, and M. Sun, "Chiral optical field generated by an annular subzone vortex phase plate," *Opt Lett* 43, 4594-4597 (2018).
9. Y. Yang, Q. Zhao, L. Liu, Y. Liu, C. Rosales-Guzmán, and C.-w. Qiu, "Manipulation of Orbital-Angular-Momentum Spectrum Using Pinhole Plates," *Physical Review Applied* 12(2019).
10. Y. Shen, X. Wang, Z. Xie, C. Min, X. Fu, Q. Liu, M. Gong, and X. Yuan, "Optical vortices 30 years on: OAM manipulation from topological charge to multiple singularities," *Light: Science & Applications* 8, 90 (2019).
11. D. Yang, Y. Li, D. Deng, J. Ye, Y. Liu, and J. Lin, "Controllable rotation of multiplexing elliptical optical vortices," *Journal of Physics D: Applied Physics* 52(2019).
12. X. Fang, H. Ren, and M. Gu, "Orbital angular momentum holography for high-security encryption," *Nature Photonics* (2019).
13. H. Zhang, X. Li, H. Ma, M. Tang, H. Li, J. Tang, and Y. Cai, "Grafted optical vortex with controllable orbital angular momentum distribution," *Optics express* 27(2019).
14. H. Ma, X. Li, H. Zhang, J. Tang, H. Li, M. Tang, J. Wang, and Y. Cai, "Optical vortex shaping via a phase jump factor," *Opt Lett* 44, 1379-1382 (2019).
15. Z. Man, Z. Xi, X. Yuan, R. E. Burge, and H. P. Urbach, "Dual Coaxial Longitudinal Polarization Vortex Structures," *Physical Review Letters* 124, 103901 (2020).
16. Y. Zhai, S. Fu, J. Zhang, Y. Lv, H. Zhou, and C. Gao, "Remote detection of a rotator based on rotational Doppler effect," *Applied Physics Express* 13(2020).
17. Z. Man, P. Meng, and S. Fu, "Creation of complex nano-interferometric field structures," *Optics Letters* 45, 37-40 (2020).

18. W. H. Campos, J. M. Fonseca, J. B. S. Mendes, M. S. Rocha, and W. A. Moura-Melo, "How light absorption modifies the radiative force on a microparticle in optical tweezers," *Applied Optics* 57, 7216-7224 (2018).
19. H. Wang, L. Tang, J. Ma, X. Zheng, D. Song, Y. Hu, Y. Li, and Z. Chen, "Synthetic optical vortex beams from the analogous trajectory change of an artificial satellite," *Photonics Research* 7(2019).
20. H. Kim, J. Park, S. W. Cho, S. Y. Lee, M. Kang, and B. Lee, "Synthesis and Dynamic Switching of Surface Plasmon Vortices with Plasmonic Vortex Lens," *Nano Letters* 10, 529-536 (2010).
21. Nir, Shitrit, Itay, Bretner, Yuri, Gorodetski, Vladimir, Kleiner, Erez, and Hasman, "Optical Spin Hall Effects in Plasmonic Chains," *Nano Letters* 11, 2038-2042 (2011).
22. L. Marrucci, "Spinning the Doppler effect," *Science* 341, 464-465 (2013).
23. M. Padgett, "A new twist on the Doppler shift," *Physics Today* 67, 58-59 (2014).
24. H. Zhou, D. Fu, J. Dong, P. Zhang, and X. Zhang, "Theoretical analysis and experimental verification on optical rotational Doppler effect," *Optics express* 24, 10050-10056 (2016).
25. Hai-Long, Zhou, Dong-Zhi, Fu, Jian-Ji, Dong, Pei, Zhang, Dong-Xu, and Chen, "Orbital angular momentum complex spectrum analyzer for vortex light based on the rotational Doppler effect," *Light Science & Applications* (2016).
26. H. L. Zhou, D. Z. Fu, J. J. Dong, P. Zhang, D. X. Chen, X. L. Cai, F. L. Li, and X. L. Zhang, "Orbital angular momentum complex spectrum analyzer for vortex light based on the rotational Doppler effect," *Light Sci Appl* 6, 16251 (2017).
27. S. Fu, T. Wang, Z. Zhang, Y. Zhai, and C. Gao, "Non-diffractive Bessel-Gauss beams for the detection of rotating object free of obstructions," *Optics express* 25, 20098-20108 (2017).
28. W. Zhang, D. Zhang, X. Qiu, and L. Chen, "Quantum remote sensing of the angular rotation of structured objects," *Physical Review A* 100, 043832 (2019).
29. J. Wang, J. Y. Yang, I. M. Fazal, N. Ahmed, Y. Yan, H. Huang, Y. Ren, Y. Yue, S. Dolinar, and M. Tur, "Terabit free-space data transmission employing orbital angular momentum multiplexing," *NATURE PHOTONICS* 6, 488-496 (2012).
30. T. Lei, M. Zhang, Y. Li, P. Jia, G. N. Liu, X. Xu, Z. Li, C. Min, J. Lin, and C. Yu, "Massive individual orbital angular momentum channels for multiplexing enabled by Dammann gratings," *Light Science & Applications* 4, e257 (2015).
31. S. Fu, Y. Zhai, H. Zhou, J. Zhang, and C. Gao, "Demonstration of free-space one-to-many multicasting link from orbital angular momentum encoding," *Optics Letters* 44, 4753 (2019).
32. M. Granata, C. Buy, R. Ward, and M. Barsuglia, "Higher-Order Laguerre-Gauss Mode Generation and Interferometry for Gravitational Wave Detectors," *Physical Review Letters* 105, 231102 (2010).
33. N. Andreas, B. Christina, and W. Benno, "Higher-order Laguerre-Gauss modes in (non-) planar four-mirror cavities for future gravitational wave detectors," *Optics Letters* 42, 751 (2017).
34. S. Qiu, T. Liu, Z. Li, C. Wang, Y. Ren, Q. Shao, and C. Xing, "Influence of lateral misalignment on the optical rotational Doppler effect," *Appl Opt* 58, 2650-2655 (2019).
35. S. Qiu, T. Liu, Y. Ren, Z. Li, C. Wang, and Q. Shao, "Detection of spinning objects at oblique light incidence using the optical rotational Doppler effect," *Optics express* 27, 24781-24792 (2019).
36. V. G. Shvedov, A. S. Desyatnikov, A. V. Rode, W. Z. Krolikowski, and Y. S. Kivshar, "Optical guiding of absorbing nanoclusters in air," *Optics express* 17, 5743-5757 (2009).
37. J. M. Hickmann, E. Fonseca, W. C. Soares, and S. Chávez-Cerda, "Unveiling a Truncated Optical Lattice Associated with a Triangular Aperture Using Light's Orbital Angular Momentum," *Physical Review Letters* 105, 053904 (2010).
38. Zhimin, Shi, Mohammad, Mirhosseini, Jessica, Margiewicz, Mehul, Malik, Freida, and Rivera, "Scan-free direct measurement of an extremely high-dimensional photonic state," *Optica* 2, 388-392 (2015).
39. G. Kulkarni, R. Sahu, O. S. Magaña-Loaiza, R. W. Boyd, and A. K. Jha, "Single-shot measurement of the orbital-angular-momentum spectrum of light," *Nature Communications* 8, 1054 (2017).
40. S. Fu, T. Wang, S. Zhang, and C. Gao, "Integrating 5×5 Dammann gratings to detect orbital angular momentum states of beams with the range of 24 to +24," *Applied Optics* 55, 1514 (2016).
41. Y. Wen, I. Chremmos, Y. Chen, J. Zhu, Y. Zhang, and S. Yu, "Spiral Transformation for High-Resolution and Efficient Sorting of Optical Vortex Modes," *Physical Review Letters* 120, 193904 (2018).
42. V. Grillo, A. H. Tavabi, F. Venturi, H. Larocque, and E. Karimi, "Measuring the orbital angular momentum spectrum of an electron beam," *Nature Communications* 8, 15536 (2017).
43. Z. Peng, S. Li, F. Xue, K. Cui, and Y. Huang, "Measuring the complex orbital angular momentum spectrum of light with a mode-matching method," *Optics Letters* 42, 1080 (2017).
44. H. L. Zhou, D. Z. Fu, J. J. Dong, P. Zhang, D. X. Chen, X. L. Cai, F. L. Li, and X. L. Zhang, "Orbital angular momentum complex spectrum analyzer for vortex light based on the rotational Doppler effect," *Light Sci Appl* 6, e16251 (2017).
45. S. Fu, S. Zhang, T. Wang, and C. Gao, "Measurement of orbital angular momentum spectra of multiplexing optical vortices," *Optics express* 24, 6240 (2016).
46. J. Pinnell, I. Nape, B. Sephton, M. A. Cox, V. Rodriguez-Fajardo, and A. Forbes, "Modal analysis of structured light with spatial light modulators: a practical tutorial," *J Opt Soc Am A Opt Image Sci Vis* 37, C146-C160 (2020).
47. A. D'Errico, R. D'Amelio, B. Piccirillo, F. Cardano, and L. Marrucci, "Measuring the complex orbital angular momentum spectrum and spatial mode decomposition of structured light beams," *Optica* 4, 1350 (2017).

48. J. M. Andersen, S. N. Alperin, A. A. Voitiv, W. G. Holtzmann, J. T. Gopinath, and M. E. Siemens, "Characterizing vortex beams from a spatial light modulator with collinear phase-shifting holography," *Applied Optics* 58, 404 (2019).
49. T. W. Clark, R. F. Offer, S. Franke-Arnold, A. S. Arnold, and N. Radwell, "Comparison of beam generation techniques using a phase only spatial light modulator," *Optics express* 24, 6249-6264 (2016).
50. C. Rosales-Guzmán and A. Forbes, "How to Shape Light with Spatial Light Modulators," (2017).
51. D. Alessio, D. Raffaele, P. Bruno, C. Filippo, and M. Lorenzo, "Measuring the complex orbital angular momentum spectrum and spatial mode decomposition of structured light beams," *Optica* 4, 1350- (2017).
52. M. Herráez, D. R. Burton, M. J. Lalor, and M. A. Gdeisat, "Fast two-dimensional phase-unwrapping algorithm based on sorting by reliability following a noncontinuous path," *Applied Optics* 41, 7437-7444 (2002).
53. K. Qian, "Two-dimensional windowed Fourier transform for fringe pattern analysis: Principles, applications and implementations," *Optics & Lasers in Engineering* 45, 304-317 (2007).
54. H. I. Sztul and R. R. Alfano, "The Poynting vector and angular momentum of Airy beams," *Optics express* 16, 9411-9416 (2008).
55. L. Torner, J. Torres, and S. Carrasco, "Digital spiral imaging," *Optics express* 13, 873-881 (2005).